Photochromic Bacteriorhodopsin Mutant with High Holographic Efficiency and Enhanced Stability via a Putative Self-Repair Mechanism

Matthew J. Ranaghan,[†] Jordan A. Greco,[‡] Nicole L. Wagner,[†] Rickinder Grewal,[†] Rekha Rangarajan,[†] Jeremy F. Koscielecki,[‡] Kevin J. Wise,[†] and Robert R. Birge*[,†,‡]

[†]Department of Molecular and Cell Biology, University of Connecticut, 91 North Eagleville Road, Storrs, Connecticut 06269, United States

[‡]Department of Chemistry, University of Connecticut, 55 North Eagleville Road, Storrs, Connecticut 06269, United States

Ⓢ *Supporting Information*

ABSTRACT: The **Q** photoproduct of bacteriorhodopsin (BR) is the basis of several biophotonic technologies that employ BR as the photoactive element. Several blue BR (bBR) mutants, generated by using directed evolution, were investigated with respect to the photochemical formation of the **Q** state. We report here a new bBR mutant, D85E/D96Q, which is capable of efficiently converting the entire sample to and from the **Q** photoproduct. At pH 8.5, where **Q** formation is optimal, the **Q** photoproduct requires 65 kJ mol^{-1} of amber

light irradiation (590 nm) for formation and 5 kJ mol^{-1} of blue light (450 nm) for reversion, respectively. The melting temperature of the resting state and **Q** photoproduct, measured via differential scanning calorimetry, is observed at 100 °C and 89 °C at pH 8.5 or 91 °C and 82 °C at pH 9.5, respectively. We hypothesize that the protein stability of D85E/D96Q compared to other blue mutants is associated with a rapid equilibrium between the blue form E85(H) and the purple form E85(−) of the protein, the latter providing enhanced structural stability. Additionally, the protein is shown to be stable and functional when suspended in an acrylamide matrix at alkaline pH. Real-time photoconversion to and from the **Q** state is also demonstrated with the immobilized protein. Finally, the holographic efficiency of an ideal thin film using the **Q** state of D85E/D96Q is calculated to be 16.7%, which is significantly better than that provided by native BR (6−8%) and presents the highest efficiency of any BR mutant to date.
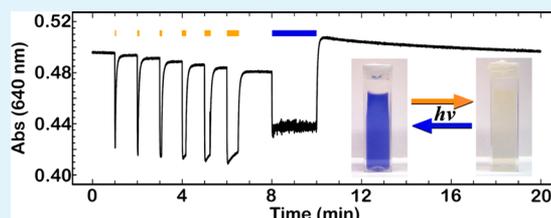
KEYWORDS: *blue bacteriorhodopsin, Q-state, stability, bionanotechnology, electro-optical materials, directed evolution*

Bacteriorhodopsin (BR) is the light-harvesting protein expressed by the salt marsh *archaeon, Halobacterium salinarum*, when the environment lacks sufficient free oxygen to permit oxidative phosphorylation as a source of energy.[1,2] This transmembrane protein contains a covalently linked chromophore, *all-trans* retinal, and is arranged in trimers within a semicrystalline lattice.[3−5] The ensemble is referred to as the purple membrane. Following the absorption of light by retinal, the light-adapted form of the protein pumps a proton across the cell membrane, thereby creating a pH gradient that then drives ATPase to synthesize ATP.[2,6] Proton pumping is achieved by a photocycle that returns to the resting state (**bR**) in roughly 10 ms at ambient temperature.[7−9] While chemical and genetic modifications of BR have been used to extend the lifetime of various intermediates in the main photocycle,[10−12] these methods have only recently produced highly stable intermediates for use of the protein in long-term data storage[13−15] and associative processors.[10,16−19] The ability to efficiently convert this photochromic protein from **bR** (λ_{max} = 570 nm) to an inactive state, known as the **Q** photoproduct (λ_{max} = 390 nm), is of interest for the successful implementation of BR into these optical devices.

The **Q** state is a photoproduct of the BR branched photocycle and remains stable for many years at ambient temperature.[20,21] The chromophore in **Q** is in a 9-*cis* configuration, which makes it an untenable candidate for binding to Lys-216 due to steric interactions with various binding site residues.[18,20,21] Bacteriorhodopsin does not form **Q** during the native photocycle, however, and requires the sequential absorption of a green photon to photoexcite the **bR** state and a red photon during the population of the **O** state (λ_{max} = 610 nm) in order to produce **Q** (Figure 1).[21] Photochemical formation of **Q** occurs with a lower quantum efficiency than the initial photoexcitation event ($\phi \sim 0.65$),[7] as measured for a deionized form of the native protein ($\phi_Q \leq 1.2 \times 10^{-4}$).[18] Hence, BR must be genetically modified to efficiently produce **Q** before the photoproduct can be utilized in protein-based technologies.[13,15−17,22]

Blue BR (bBR) membranes contain modified proteins that exhibit an *O-like* resting state (**bR$_B$**; $\lambda_{max} \sim 603$ nm) and are
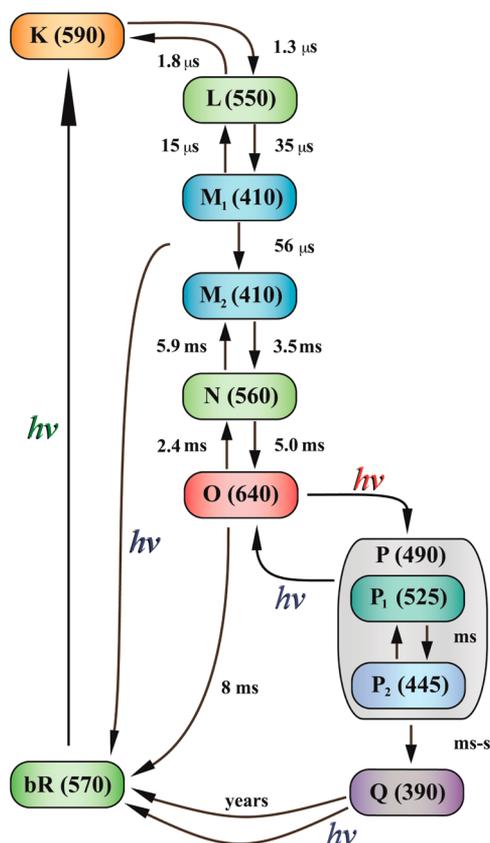
Figure 1. Main and branched photocycles of native BR. The kinetic lifetimes of the BR photostates, with the respective absorption maxima (in nanometers) in parentheses, are from refs 20 and 67.

produced by either mutagenesis or low pH-induced protonation of the Asp-85 residue.[18,23−28] The bBR form of the protein is a bistable photochrome that is long known to efficiently produce the *pink membrane* ($\lambda_{max} \sim 490$ nm), a 9-*cis* precursor to the **Q** photoproduct.[25,29] Chemical bBR membranes are generated by acidification with a strong acid or deionization of the bulk protein;[30−32] however, such chemical modification affects the entire protein structure and can significantly destabilize the protein conformation.[33−35] The phototransformations of these bBR membranes to the **Q** photoproduct are also characterized by poor quantum efficiencies ($\phi_Q \sim 2 \times 10^{-4}$ to 7×10^{-3}).[18,36] Conversely, mutational manipulation of BR results in a more localized perturbation of the protein structure and provides a more advantageous method for producing stable bBR membranes. Novel methods in genetic engineering, including directed evolution, allow the photophysical properties of BR to be tailored for specific applications. Directed evolution was used to enhance the ability of BR to form the **Q** photoproduct for use as a molecular medium in optical devices.[22] Of the 1,604 unique BR mutants characterized in the directed evolution search, eleven qualify as bBR membranes, and one mutant (D85E/D96Q) exhibits both high stability and the ability to fully switch between the **bR$_B$** and **Q** photostates. Below, we describe the development of novel bBR mutants via directed evolution, the biophysical characterization of the D85E/D96Q mutant to optimize **Q** formation, and demonstrate the ability to cycle the immobilized D85E/D96Q protein between the **bR$_B$** and **Q** states in real-time. Calculation of the holographic efficiency of the **bR$_B$/Q** pair in an ideal thin film shows a

marked improvement over similar films that use the **bR** and **M** ($\lambda_{max} \sim 410$ nm) photostates of native BR[37,38] or the **bR/Q** pair in the high **Q**-forming BR mutant,V49A.[22]

We note that the letter Q is used in several contexts throughout this paper and define them here for clarity: **Q** represents the **Q** photoproduct of the branched BR photocycle, Q_{total} represents a quality score used to rank BR mutants created during directed evolution, and Q in D85E/D96Q represents the amino acid glutamic acid.

■ METHODS AND MATERIALS

Chemicals and Buffers. All chemicals were purchased from Thermo Fisher Scientific, Inc. (Pittsburg, PA) or Sigma Aldrich (St. Louis, MO). Buffers used for pH investigations were 50 mM phosphate for pH 6.5 to 7.5, 50 mM tris(hydroxymethyl)methyl-3-aminopropanesulfonic acid (TAPS) for pH 8.0 and 8.5, 50 mM glycine for pH 9.0 and 9.5, or 50 mM 3-(cyclohexylamino)propanesulfonic acid (CAPS) for pH 10.0 and 10.5.

Strain Generation, Library Construction, and Protein Preparation. The methods for strain generation, construction of the mutant library, and the large-scale preparation and purification of bBR mutants are described in the Supporting Information. All experiments used only the high-density form of bBR proteins (see the Supporting Information methods and Figures S1 and S2), unless noted otherwise.

Calculation of the D85E/D96Q Molar Extinction Coefficient. The molar extinction coefficient (ε) of the **bR$_B$** and **Q** states of bBR mutant D85E/D96Q was experimentally determined at alkaline pH. This characterization was necessary for experiments that were conducted at pH 8.5, 9.5, and pH 10.5 to correct for the blue-shifted λ_{max} at alkaline pH (Figure S3). Buffer exchange was done three times by using ultracentrifugation (50,000 rpm for 20 min at 4 °C), with resuspension of the protein in the appropriate buffer and equilibration for 30 min at ambient temperature after each exchange. The ε was experimentally determined by manipulation of the Beer-Lambert law using spectra of the **bR$_B$** and **Q** states at each pH. Light-adaptation of either the **bR$_B$** or **Q** states was done using either white light (300 W) for 1 h at ambient temperature for the **bR$_B$** state or red light (>640 nm; 100 mW cm^{-2}) overnight at 30 °C induce the **Q** photoproduct.

Preparation of the Q Photoproduct. A 1 mg mL^{-1} sample of bBR membrane was prepared at an alkaline pH in a clear microcentrifuge tube (Thermo Fisher Scientific, Inc.). The sample was then placed under red LED irradiation (100 mW cm^{-2}; >640 nm) overnight at 30 °C. Upon completion, an aliquot was taken for analysis before the sample was wrapped in foil and stored at 4 °C until use.

Absorption Spectroscopy. Spectroscopic investigations were conducted with a Varian Cary 50 UV-visible spectrophotometer (Palo Alta, CA). Measurements were collected at ambient temperature, unless noted otherwise, in either distilled water (Millipore, Billerica, MA) or buffer.

Differential Scanning Calorimetry. All calorimetric experiments were done with 1 mg mL^{-1} protein using a Microcal VP-DSC (Amherst, MA). Dialysis of all samples versus three one-liter volumes of the appropriate buffer was determined to generate the most reproducible data. The **Q** photoproduct was produced as described above, and, because it is light sensitive, all manipulation was conducted under dim red light.

Kinetic DSC experiments were conducted at various scanning rates (30 to 90 K h^{-1}) based on experimental design. The *melting temperature* (T_M) of transitions within DSC thermograms were extracted and fit to the kinetic equation

$$\ln\left(\frac{v}{T_M^2}\right) = const - \frac{E_{APP}}{RT_M}$$

(1)

where v is the scan rate (K min^{-1}), T_M is the melting temperature (K) from DSC thermograms, E_{APP} is the apparent energy of thermal denaturation (kJ mol^{-1}), and R is the gas constant (8.314 J mol^{-1} K^{-1}).[39,40]
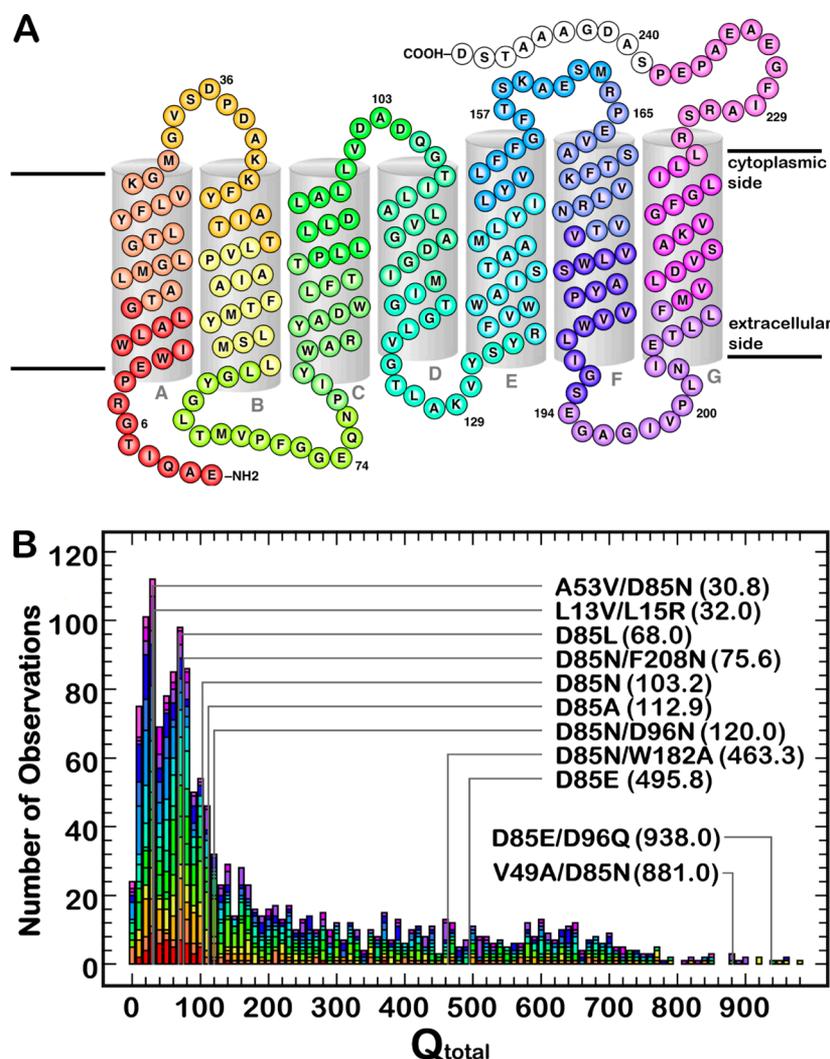
Figure 2. (A) Two-dimensional map of native BR. The color-coded divisions of the protein represent the target regions used for mutagenesis. These regions contain the following sets of residues (numerically): 1-16; 17-32; 33-47; 48-61; 62-76; 77-90; 91-104; 105-118; 119-133; 134-148; 149-163; 164-178; 179-193; 194-208; 209-223; 224-238. (B) Histogram of bacteriorhodopsin mutants created throughout six rounds of directed evolution to enhance the accessibility of the **Q** photoproduct. The Q_{total} values of each bBR mutant are shown in parentheses.

Determining the Activation Energy for Q Formation and Reversion. Specialized equipment was designed to measure the ability of the D85E/D96Q mutant to switch between the **bR$_B$** and **Q** photostates at alkaline pH. The experimental setup suspends a set of four amber Luxeon III Lambertian LEDs (590 nm, 0.3 mW cm^{-2}) or three UV mcd LEDs (390 nm, 0.02 mW cm^{-2}) above the sample holder of a Cary 50 UV-visible spectrophotometer with a peltier sample cell. The experiment began by collecting an initial set of spectra of D85E/D96Q in either the **bR$_B$** or **Q** state (OD ∼ 0.1) at t = 0 min before turning on the LED device and monitoring light-induced changes by collecting spectra in three stages (1 min intervals to 10 min; 5 min intervals to 50 min; 30 min intervals to 300 min). The kinetic data were then fit to a first order exponential decay rate

$$A_t = A_\infty + (A_0 - A_\infty)e^{-kt} \qquad (2)$$

where A_t is the absorbance at time t, A_∞ is the absorbance at time infinity, A_0 is the absorbance at time zero, k is the decay or rise rate (min^{-1}), and t is the time (min). Experiments were done in triplicate at temperatures between 36 and 50 °C and then fit to an Arrhenius plot to approximate the activation energy for the transition.

Preparation of Hydrated Polymer/bBR Cuvettes. Bacteriorhodopsin was immobilized within a 5% polyacrylamide matrix that was buffered with 50 mM TAPS (pH 8.5). The optical density (OD) of each sample was approximately 1 at the absorption maximum of the

bR$_B$ state. To prepare the polymer-based cuvettes, the BR solution was first sonicated on ice for 60 seconds using 10-second intervals, to ensure homogeneity, and was then filtered using 5 μm filter paper into a sterile falcon tube. Ammonium persulfate (400 μL) was added, and the solution was degassed for 30 minutes. The protein solution was transferred equally into either 4.0 mL or 1.5 mL methacrylate cuvettes (Plastibrand Cuvettes, Fisher Scientific, Inc.) that were optically transparent on all sides. Next, 0.5% (v v^{-1}) tetramethylethylenediamine (TEMED; Fisher Bioreagents, electrophoresis grade, assay 97%) was added to each cuvette, mixed well, and allowed to polymerize at ambient temperature. A 15% (w v^{-1}) polyvinyl alcohol (PVA; Aldrich, 99+% hydrolyzed, avg. MW 89-98,000) solution, which was degassed and buffered with TAPS, was applied to fill the remaining headspace within the cuvette. The cap was sealed using a chemically inert adhesive and was wrapped with Parafilm to prevent condensation within the cuvette.

Real-Time Q Formation Experiments. Specialized equipment was designed to measure the ability of the D85E/D96Q mutant to switch between the **bR$_B$** and **Q** photostates. The experimental setup is comprised of a Cary 50 UV-visible spectrophotometer, a modified sample cell holder with holes for LEDs on either side of the cuvette, one royal blue (0.3 mW cm^{-2}; 450 nm) and one amber (0.2 mW cm^{-2}; 590 nm) Luxeon III LED, and a 1014 Phidget (Alberta, Canada) board. The on/off times of the LEDs were computer controlled via a

2801

dx.doi.org/10.1021/am405363z | ACS Appl. Mater. Interfaces 2014, 6, 2799−2808

USB connection to the Phidget board, which uses electrical relays. The Phidget board was driven by *in-house* software written for MathScriptor (www.mathscriptor.org). The LEDs were powered at 75% to stabilize the illumination and prevent overdriving of the LEDs.

Holographic Efficiency Calculation. The holographic performance of BR is associated with the large change in refractive index, which accompanies the population of spectrally shifted intermediates. A theoretical analysis of the holographic efficiency associated with the photoconversion between the bR_B and **Q** states in an ideal, field-oriented film was done based on the solution spectra of D85E/D96Q at pH 8.5. A Kramers-Kronig transformation of the spectra yields the relationship between the absorption spectrum and refractive index changes of a modulated BR film. Kogelnik's coupled wave theory for thick holographic gratings was used to predict the holographic diffraction efficiency.[41] Hydrated, polymer-based BR films (20−100 μm) have been previously developed and implemented as holographic media in biophotonic devices.[10,11,15,19,37,42−44] Films based on the native protein function as volume transmission holograms due to the small size of the protein (50 nm diameter) relative to the activating light wavelength (570 nm) and have been experimentally shown to perform at a resolution that approaches 5000 lines/mm.[45] The diffraction efficiency for a film of native BR (OD = 6) with a 1:1 mixture of the **bR** and **M** states was measured as ∼8% at 640 nm, which is close to the ∼10% efficiency predicted by using the Kramers-Kronig relationship and Kogelnik approximation.[46] When the observed and calculated data are compared, the Kogelnik theory is often found to overestimate the actual performance by roughly 20%.[46,47]

While the maximum diffraction efficiency of an absorption grating is 3.7%,[41] mixed absorption and refraction holograms facilitated by the photophysical properties of BR can have diffraction efficiencies that approach 100%.[38] The equations used for the Kramers-Kronig relationship and Kogelnik approximation are provided in the Supporting Information and have been previously used to describe the **bR**→**M** photoreaction of BR.[19,47,48] In addition to the bR_B and **Q** state analysis of D85E/D96Q, we performed the calculation for the **bR**/**Q** photochromic pair of the high **Q**-forming mutant, V49A,[22] using solution spectra collected at pH 8.5. All samples were prepared, and all spectra were collected as described above.

RESULTS AND DISCUSSION

Directed Evolution of BR. Many of the current biophotonic technologies that utilize BR as a photochromic material use the transient **M** photostate (see ref 49 and references therein). The **Q** photoproduct can substitute for **M** in many of these applications with the added advantage of being a stable photoproduct with a more blue-sifted λ_{max} that yields better separation of the photochromic pair. However, formation of the **Q** photoproduct is not beneficial to *H. salinarum* and thus is produced in minimal amounts within the native protein. Six rounds of directed evolution were performed to enhance the **Q** formation properties of BR.[22] A quality score (Q_{total}) was experimentally measured to assess the ability of each mutant to form and revert from the **Q** photoproduct. Native BR exhibits a Q_{total} of ∼15 (pH 7), and higher values indicate an improvement in **bR**→**Q** and/or **Q**→**bR** photo-reactions, with the highest Q_{total} score being 977 for a quadruple mutant of BR. Of the 1604 unique mutants characterized throughout the six rounds of mutagenesis, eleven mutants with red-shifted absorption maxima (λ_{max} = 585−610 nm) were identified (Figure 2). These bBR mutants all contain either one or two mutations to the native protein sequence. Attempts to introduce additional mutations to double bBR mutants resulted in either no or significantly low yields of protein.

Two bBR mutants had Q_{total} values greater than 850: V49A/D85N and D85E/D96Q (Figure 2). The D85E/D96Q mutant exhibited the greatest **Q** formation ability of any bBR mutant

and expressed well (2-4 mg per liter of culture) under preparation methods described in the Supporting Information. While the conditions particular to the formation of **Q** are characterized below, we note that D85E/D96Q is capable of converting the entire sample (>99% efficiency) to the **Q** state at slightly alkaline pH (Figure 3, *circles*). We also note that the
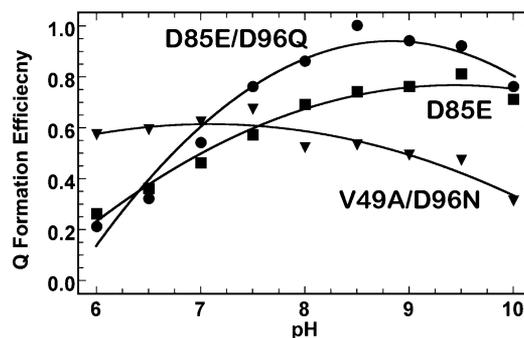
Figure 3. The pH dependence of **Q** formation for three bBR mutants with the greatest Q_{total} values from Figure 2.

enhanced sensitivity and holographic properties of V49A/D85N are already known,[28,50] but this mutant is reported to have <1% conversion to the **Q** state.[28] Conversely, we find that V49A/D85N can produce **Q** with 30−60% efficiency, depending on the pH, when immobilized in a polyacrylamide matrix (Figure 3, *inverted triangles*). However, the V49A/D85N mutant is not capable of full conversion to a stable **Q** photoproduct, and the subsequent sections will thus characterize **Q** using D85E/D96Q.

Spectral Titration of D85E/D96Q. Interactions within the active site of BR mutants are conventionally characterized via the *purple-to-blue* transition. This transition represents the physical conversion of the protein pigmentation (i.e., λ_{max}), as is defined by the protonation state of the D85 counterion.[27,51,52] The native protein exhibits a pK_A of ∼3 for this shift,[53] where mutational bBR membranes exhibit a blue pigmentation at neutral pH and undergo a *blue-to-purple* transition with a pK_A > 7.[26,54,55]

Titration of D85E/D96Q reveals a pK_A at approximately pH 9.7 (Figure S3). This value is close to the value reported for the D85E mutant (9.4) and also represents the titration of the Schiff base counterion at position 85.[51,56] Perturbation of the active site geometry is well documented to control the pK_A of the Schiff base and thus the λ_{max} of the protein.[26,27] Nevertheless, we find that titration of D85E/D96Q caused an analogous blue-shift of the λ_{max} to that of the D85E mutant,[51] where both mutants absorb around 530 nm at pH 11. This blue-shifted species, which is the 'purple' form of D85E/D96Q, forms above the pK_A and indicates the formation and stabilization of a deprotonated counterion residue E85(-). Moreover, pH values below the pK_A stabilize the protonated form of E85, E85(H), which is the red-shifted species that is consistent with the acid blue membrane.[32,35] Hence, the observed broad absorbance of D85E/D96Q likely represents a dynamic equilibrium between E85(H) and E85(-), which has implications on both protein stability and **Q** formation and reversion (see below). The D85E/D96Q mutant irreversibly denatured at highly alkaline pH (i.e., >11), as evidenced by a yellow hue of the sample ($\lambda_{max} \approx 360$ nm) and inability to revert the protein with the addition of acid. Alkaline

2802

dx.doi.org/10.1021/am405363z | *ACS Appl. Mater. Interfaces* 2014, 6, 2799−2808

denaturation of D85E/D96Q is consistent with earlier reports of other mutant bBR membranes.[51,56]

Thermal Stability of D85E/D96Q. The thermal stability of native BR is conventionally quantified by measuring two thermal transitions, which are centered at 80 °C and 100 °C, in DSC thermograms.[57] In native BR, these transitions represent a reversible thermal relaxation of the protein and irreversible denaturation, respectively.[58−60] The irreversible thermal transition is observed to be within 7 °C of native BR for all tested bBR mutants (Figure S4A), indicating that there is minimal perturbation of the protein structure. These T_M data can be fit to eq 1 by collecting thermograms with varied heating rates, which estimates the apparent energy (E_{APP}) required for thermal denaturation of the protein. This method removes the scan rate dependence of the T_M, because BR is a kinetically stabilized protein,[40] and is a better metric of stability than a single T_M value. The E_{APP} of both D85E and D85E/D96Q are comparably stable to native BR, where both D85N and V49A/ D85N are not (Figures S4, B and C).

We hypothesize that the *native-like* stability of D85E and D85E/D96Q results, at least in part, via a *self-repair mechanism* that is related to the protonation state of the counterion residue (see above). While this mechanism remains to be fully understood, it is clear that D85E and D85E/D96Q are more stable than chemically modified bBR membranes[34,61] and other bBR mutants (Figure S4 and ref 62). This observation supports a role for the counterion residue being transiently charged versus completely neutral, which is the case for the D85N mutants. We cannot say whether this stability results from a rearrangement of the hydrogen-bonded network within BR or from proton transfer to a nearby acceptor at this time; however, the key is likely a fast equilibrium of the photochemically active blue form E85(H) with a highly stable purple form E85(−) that is accessed on a millisecond time scale to repair any thermal predenaturation of the blue form. The relative amount of purple to blue form is controlled via pH (Figure 3), but this protein appears to be very stable in the range 6 < pH < 10, which suggests that the purple form need not be dominant to provide the desired thermal and photochemical stability.

Optimal Q Formation Occurs at Alkaline pH. The active site of native BR is not amenable to the formation of the 9-*cis* retinal configuration.[18] Under sufficient red-light illumination, however, D85E/D96Q produces significant amounts of the **Q** photoproduct at alkaline pH. Figure 3, in combination with Figure S3, illustrates the importance of the protonation state of the residues that direct **Q** formation within the active site of BR. Alkaline pH, especially pH 8.5 (see below), is optimal for hydrolyzing the 9-*cis* retinal within the D85E/D96Q active site. Water is essential for the hydrolysis event during the **P→Q** transition, and, if the protein is dehydrated, formation of the **P** state is favored with little or no **Q** production.[20]

Formation of **Q** coincides with the spectral shift of the **bR$_B$** λ_{max} at alkaline pH. The spectral shift of the D85E/D96Q λ_{max} spans approximately 80 nm between pH 8.5 and 10.5 and determining the ε for these experimental conditions was necessary to characterize the **Q** state. Hence, the ε was established at three pH values (8.5, 9.5, and 10.5) to properly investigate the photophysical properties of **Q** formation (Table 1). We note that the ε values determined for the D85E/D96Q **Q** photoproduct at alkaline pH differ from the published value, which use native BR, of 33,000 M^{-1} cm^{-1}.[20] This difference not only is most likely from alterations within the binding site of the D85E/D96Q mutant but also may result from the varied

Table 1. Summary of the Spectral Properties of bBR Mutant D85E/D96Q

photostate	pH	λ_{max} (nm)	ε (M^{-1} cm^{-1})
resting state (**bR$_B$**)	water	608	43,000 ± 2,000
	8.5	608	34,000 ± 550
	9.5	565	28,500 ± 1,900
	10.5	530	27,000 ± 1,200
Q photoproduct	8.5	390	40,000 ± 650
	9.5	385	40,000 ± 700
	10.5	385	37,000 ± 1,100

hydration, which is vital for forming the **Q** photoproduct, in the cited work.

Real-time spectral analysis of **Q** formation at alkaline pH was conducted under continuous illumination with amber light (Figure 4). These data show the conversion of the *O-like* **bR$_B$**
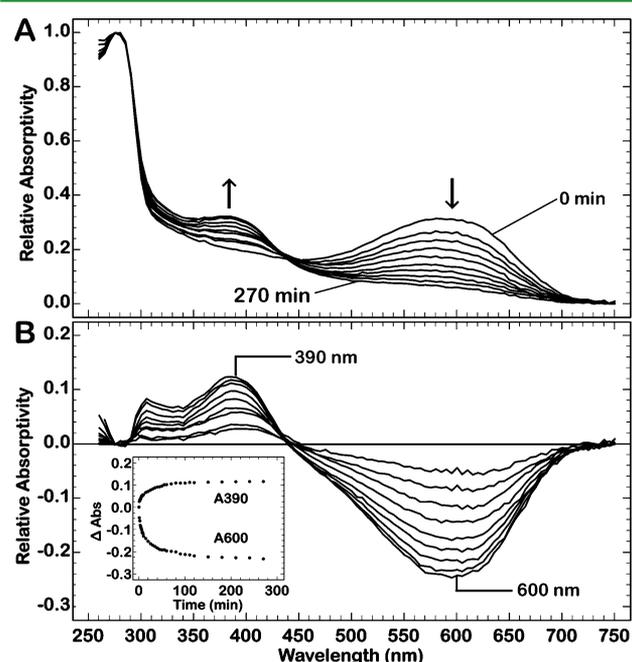
Figure 4. (A) Representative spectra for illuminating D85E/D96Q with continuous amber light at pH 8.5. These data were collected at 58 °C and used for determining the activation energy of the **bR$_B$→Q** photoreaction (see Figure S5). (B) Difference spectra of Figure 4A. Kinetic traces of photoconversion are shown in the inset image and were fit to eq 2.

state to a blue-shifted photoproduct that is centered at ∼390 nm. To confirm that the blue-shifted absorbance is the **Q** state, and not a denatured form of the protein, the sample was subjected to continuous blue light irradiation.[63] This illumination converts the **Q** photoproduct back to the *O-like* **bR$_B$** state with a rate that is influenced by the solution pH and temperature (data not shown). The latter dependence allows for determination of the activation energy barrier of thermal denaturation by Arrhenius treatment of the kinetic data (Figure S5). Energies were determined at pH 8.5 and 9.5 because these conditions are the most favorable for **Q** formation (Figure 3). Amber (590 nm) LEDs, rather than red (>640 nm), were used for better coupling with the protein at both pH values. For the **bR$_B$→Q** and **Q→bR$_B$** photoconversions, these values are 65 kJ mol^{-1} and 5 kJ mol^{-1} for pH 8.5 and 80 kJ mol^{-1} and 40 kJ mol^{-1} for pH 9.5, respectively. Activation energies were not

2803

dx.doi.org/10.1021/am405363z | *ACS Appl. Mater. Interfaces* 2014, 6, 2799−2808

investigated at pH 10.5 because the protein often denatured during the course of the experiment.

The thermal denaturation of native BR is sensitive to alkaline pH.[64] Because formation of **Q** required such an environment (Figure 3), understanding how alkaline pH affected the thermal stability of D85E/D96Q was essential before any practical application of the protein. We find that the irreversible T_M of the **bR$_B$** state (Figure S6A) and **Q** photoproduct (Figure S6B) decrease with increasing pH. This sensitivity is similar to that of native BR.[64] Optimal stability of D85E/D96Q was observed at pH 8.5, in which the thermogram in the **bR$_B$** state is similar to that of native BR. Despite an 11 °C decrease in the T_M, the **Q** photoproduct also exhibited a high level of stability at this pH. The E_{APP} was determined for D85E/D96Q at pH 8.5 and 9.5 (Figure S7). For the **bR$_B$** and **Q** conformations, these values are 770 and 520 kJ mol^{-1} for pH 8.5 and 100 and 150 kJ mol^{-1} for pH 9.5, respectively. These data show that D85E/D96Q is significantly destabilized above pH 8.5, despite an increased energy barrier for the **Q→bR$_B$** from 5 to 40 kJ mol^{-1}. Hence, optimal stability of and photoconversion between the **bR$_B$** and **Q** states is observed around pH 8.5 (Table 2). Most importantly, however, is that the **Q** photoproduct is comparably stable to the **bR$_B$** state and itself does not have deleterious effects on the stability of the protein.

Table 2. Summary of the Physical Properties of bBR Mutant D85E/D96Q at Neutral and Alkaline pH

photostate	pH	E_A (kJ mol^{-1})^a	T_M (°C)^b	E_{APP} (kJ mol^{-1})
resting state (**bR$_B$**)	water	nd^c	98	1050
	8.5	65	100	770
	9.5	80	91	100
	10.5	nd^c	78	nd^c
Q photoproduct	8.5	5	89	520
	9.5	40	82	150
	10.5	nd^c	65	nd^c

^{a}Activation energy for the **bR$_B$→Q** or **Q→bR$_B$** photoconversion. ^{b}The T_Ms represent values collected at 90 K h^{-1}. ^{c}nd = not determined.

Application in Biophotonic Devices. Optical memories can use either dry or hydrated suspensions of the protein.[10,15,18,28] Formation of the **Q** photoproduct requires hydrolysis of the Schiff base linkage between the protein and the 9-*cis* retinal.[20,21] We therefore investigated whether D85E/D96Q was useful in devices by suspending the protein in a hydrated polyacrylamide matrix. Such devices have been proposed for the storage and manipulation of data and offer a simple assessment of this quality.[13,15]

The left inset image of Figure 5 shows hydrated suspensions with the mutant protein in either the **bR$_B$** or **Q** photostate. Both samples were prepared at pH 8.5, which is the best pair for **bR$_B$/Q** cyclicity and stability, with an OD of ~1 at 600 nm. One sample was then illuminated with continuous red light for 16 h to ensure complete formation of the **Q** photoproduct. Spectral analysis of these samples detected the photochemical transition to the **Q** photoproduct. Optical clarity was also maintained, as evidenced by the minimal absorbance at high wavelengths (>700 nm) during the photoconversion and by no denaturation of the protein following immobilization within the polyacrylamide matrix.

Real-time cycling between the **bR$_B$** and **Q** states was also demonstrated by subjecting the sample to pulses of amber (590 nm) and royal blue (450 nm) light (Figure 6). Illumination
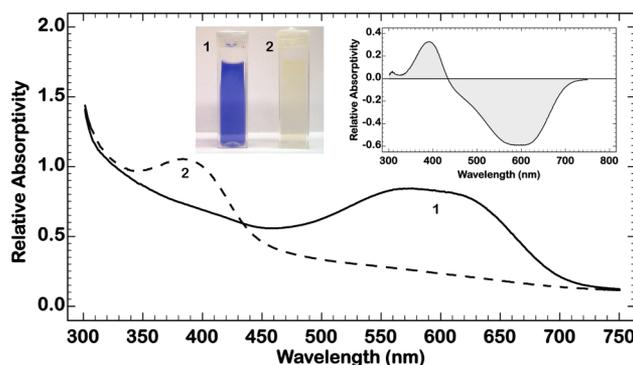
Figure 5. Absorbance spectra of the acrylamide cubes containing D85E/D96Q in the **bR$_B$** state (*solid line*) or **Q** state (*dashed line*). The left inset image is a photograph of cubes containing either the (*1*) **bR$_B$** state or (*2*) **Q** photoproduct of D85E/D96Q in a buffered (pH 8.5) polyacrylamide gel. The right inset image shows the difference spectra of D85E/D96Q spectra after illumination with (>640 nm; ~100 mW cm^{-2}) light for complete conversion after 16 h.

using the amber or royal blue LEDs resulted in a decrease or increase of the baseline at 640 nm, respectively. This wavelength is used to monitor the red-shifted component of the **bR$_B$** state as the protein converted to and from the **Q** photoproduct. Formation of **Q** was confirmed by the lasting blue-shifted absorbance at ~390 nm after the protein relaxes during the dark period that follows illumination (Figure 6B). Blue irradiation reset the baseline at 640 nm by driving the **Q→bR$_B$** photoreaction (Figure 6, A and C). While reversion of the protein to the **bR$_B$** state initially produced an increase in the postillumination baseline, this absorbance slowly decayed to the pre-experiment baseline within several minutes. This slow decay corresponds to the formation of a long-lived, red-shifted photointermediate (λ_{max} = 620 nm), presumably an **O** state, that then relaxed to the **bR$_B$** resting state of D85E/D96Q. The photoresponse of the immobilized protein to variable pulses of light over the course of several continuous experiments is further demonstrated in Figure S8.

Holographic Efficiency of Q. The blue-shift associated with **Q** also has application in protein-based associative memories, which traditionally use the refractive index change of the **bR→M** photoreaction for real-time holography.[11,15] Specifically, **Q** has two advantages over **M** in such applications. First, the **Q** photoproduct is stable for years,[20] while the longest lived **M** state exists for ~750 ms in the D96N mutant.[65] Second, **Q** is more blue-shifted than **M** by ~20 nm, which increases the spectral separation of the photochromic pair. However, the efficient formation of **Q** has only recently been realized through significant mutagenesis of BR.[22] This achievement now allows us to calculate the holographic efficiency of BR mutants using experimental data.

The holographic efficiency of D85E/D96Q was calculated from solution spectra for an ideal film with an OD of ~5 at 280 nm (OD$_{603}$ ~ 1.9) (Figure 7A). The maximal diffraction efficiency of such a film is 16.7% at 700 nm, which is notably improved over the 6−8% observed for native BR.[15,37,38] It is also improved over the 4% efficiency of V49A/D85N bBR, which uses **P** (λ_{max} = 480 nm) as the blue-shifted species.[28] This observation means the **bR$_B$/Q** states of D85E/D96Q can improve the signal-to-noise of a holographic film 2−3 times over the **bR/M** pair of a native BR film and 3−4 times over the **bR$_B$/P** pair of V49A/D85N.
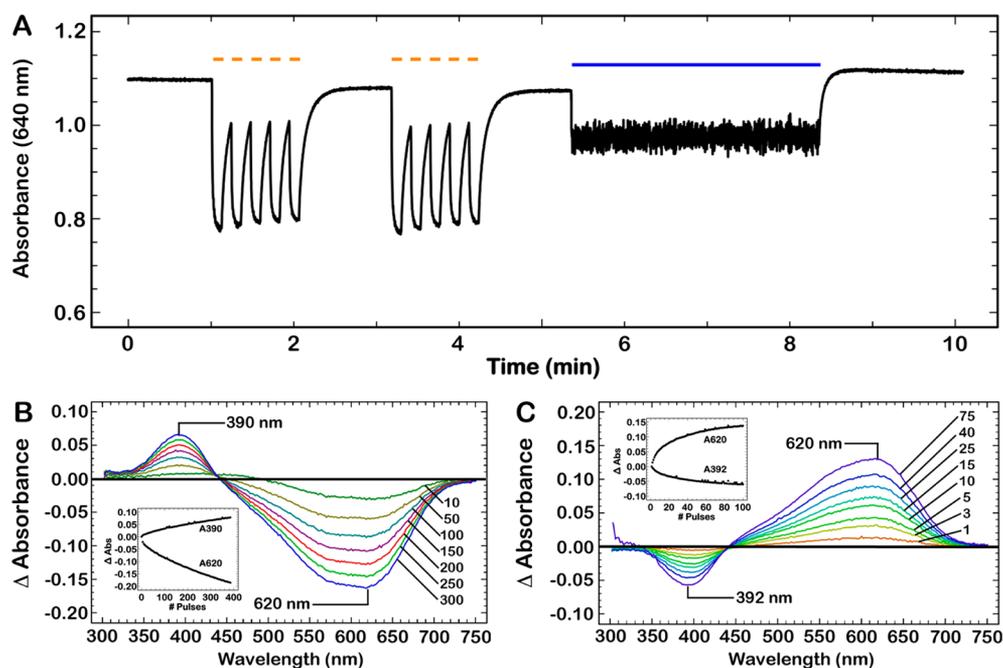
Figure 6. Illumination of D85E/D96Q, which is suspended in a buffered (pH 8.5) polyacrylamide gel, with amber (590 nm) or royal blue (450 nm) light demonstrates how the protein responds to LED illumination. (A) Real-time changes in the red-shifted absorbance band (640 nm) of the immobilized protein. Amber illumination consists of two sets of five 15-second pulses with each pulse followed by 5 seconds of dark time. Each set of pulses is followed by one minute of dark time to allow relaxation of the protein to the bR_B state if unconverted to the **Q** photoproduct. Two minutes of blue illumination are included to drive the **Q**→bR_B photoconversion and reset the A_{640} baseline. (B) Difference spectra for the bR_B→**Q** photoconversion, which are subtracted from spectra of the light-adapted protein. All spectra were collected during the long dark period following each set of five amber illuminations. The number of 15-second flashes required to produce each spectra are shown on the right side of the image. The kinetics of photoconversion are shown in the inset image for the absorption maxima and minima. (C) Data are of difference spectra for the **Q**→bR_B photoconversion and are subtracted from the spectra of D85E/D96Q after 385 15-second amber pulses. All spectra were collected during a 30 second dark period following each one second blue illumination. The number of flashes required to produce each spectra are denoted on the right side of the image. The kinetics of photoconversion are shown in the inset image for the absorption maxima and minima.

We next calculated the holographic efficiency for the **bR/Q** states of V49A, a 'purple' BR mutant capable of fully forming **Q**,[22] in order to compare it with that of D85E/D96Q. An ideal film with an OD_{280} of ~5 (OD_{570} of ~2.4) will yield a diffraction efficiency of 12.5% at 650 nm (Figure 7B), which improves the diffraction efficiency 1.5−2 times over the **bR/M** pair of a native BR. This improvement, while significant, is less than that of D85E/D96Q due to the increased spectral separation between the bR_B and **Q** states. While both proteins offer an improved holographic efficiency, D85E/D96Q exhibits the highest efficiency of any BR mutant explored to date.[10,28,37,50,66]

■ COMMENTS AND CONCLUSIONS

We report here the first bBR mutant to exhibit efficient conversion of the entire sample to and from the **Q** photoproduct. The thermal and photochemical stability of native BR makes it well-suited for application in biophotonic technologies, and this stability is not lost in the D85E/D96Q mutant. This mutant, in particular, also exhibits the highest conversion levels to the **Q** photoproduct of any bBR mutant created to date. The protein structure is partially weakened, however, under the alkaline conditions required for the formation of the **Q** photoproduct. Optimal stability and formation of **Q** is determined to occur around pH 8.5 in an aqueous environment. We hypothesize that the general stability of D85E/D96Q derives from the rapid interconversion of the protonated blue form, E85(H), and the deprotonated purple

form, E85(−), of the mutant. The barrier to proton transfer is very small, and thus this equilibrium is established within seconds, if not milliseconds. Rapid equilibration between these species serves to stabilize the blue membrane form, E85(H), and is likely responsible for stabilizing the ensemble.

Suspension of D85E/D96Q in a polyacrylamide matrix, buffered at pH 8.5, does not inhibit the formation of **Q** under the conditions optimized for the aqueous sample. Furthermore, the **Q** state is the only true photoproduct of the BR photocycle and, because it is infinitely longer-lived than the **M**[65] or **P**[18] photostates, it is ideal for long-term storage of binary data or holographic associative processing.[15] Real-time cycling of the bR_B and **Q** states of immobilized D85E/D96Q with amber and blue light demonstrates this feature. The increased spectral separation between the photochromic pair, **bR/Q**, and a high holographic efficiency of D85E/D96Q also surpasses the efficiency of all protein-based holographic media investigated to date. The coupling of this efficient photochromism with the uniquely enhanced thermal stability of D85E/D96Q dramatically improves the viability of using bBR mutants in protein-based optical computing (e.g., permanent data storage, real-time holographic data processing). Following the success of immobilizing the protein within a hydrated polymer matrix and the demonstration of repeatable photoconversion in this environment, we are now eager to investigate the application of D85E/D96Q as a photochromic material and further establish the optical and hardware requirements to harness this efficiency in various biophotonic architectures.
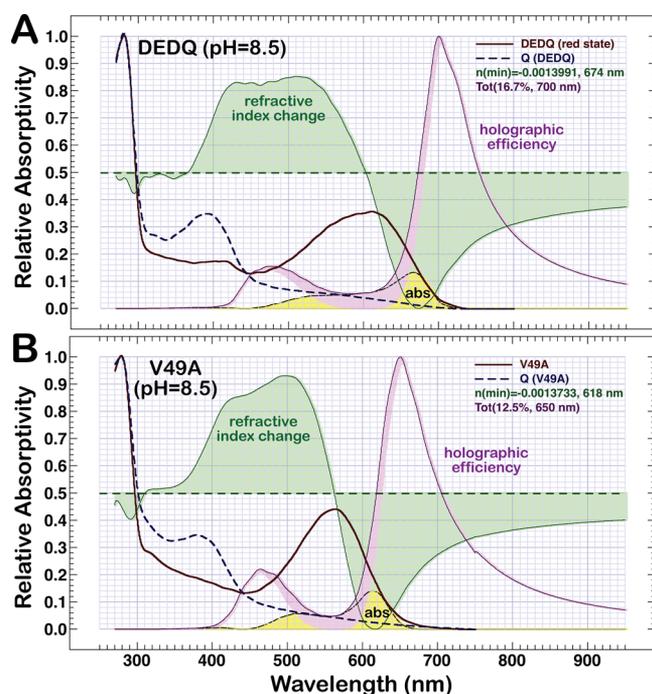
Figure 7. Calculated wavelength dependence of the holographic efficiency for D85E/D96Q (A) and V49A (B) BR using the Kramers-Kronig transformation and Kogelnik equations. The holographic efficiency (purple line) was calculated for 100% conversion of state 1 (bR_B or bR; thick red line) to state 2 (Q; dotted blue line) in a 0.01 cm thin film with an OD of 5 at 280 nm. A 10° write angle was used with a write wavelength of 532 nm. The refractive index change (shaded green line) and holographic efficiency are normalized to their maximal values. All spectra represent data collected at ambient temperature.

■ ASSOCIATED CONTENT

ⓢ Supporting Information

(1) Methods for enhancing the **Q** forming abilities of BR using directed evolution, (2) methods for preparing and characterizing the high-density D85E/D96Q protein, (3) the calculations for the theoretical holographic properties of BR thin-films using the Kramers-Kronig Transformation and Kogelnik's Coupled Wave Theory, (4) a table describing the primers used to generate bBR mutants, (5) a figure showing a typical sucrose gradient used to purify the high-density protein, (6) a figure showing the electronic absorbance spectra and DSC thermograms of the low- and high-density D85E/D96Q proteins, (7) a figure showing the electronic absorption spectra and difference spectra of D85E/D96Q when titrated from pH 8 to 11, (8) a figure that shows DSC thermograms and determines the E_{APP} of several bBR mutants in dH$_2$O, (9) a figure showing the Arrhenius plots of D85E/D96Q photoconversion from **bR$_B$→ Q** and **Q→bR$_B$** at alkaline pH, (10) a figure showing DSC thermograms of the **bR$_B$** and **Q** states of D85E/D96Q at pH 8.5 and 9.5, (11) a figure that determines the E_{APP} of D85E/D96Q at alkaline pH, (12) a figure that demonstrates the real-time cycling of D85E/D96Q between the **bR$_B$** and **Q** states when immobilized in a buffered polyacrylamide matrix, and (13) references for Supporting Information. This material is available free of charge via the Internet at http://pubs.acs.org.

■ AUTHOR INFORMATION

Corresponding Author

*Phone: 860 486-6720. Fax: 860 486-2981. E-mail: rbirge@ uconn.edu.

Notes

The authors declare no competing financial interest.

■ REFERENCES

(1) Oesterhelt, D.; Stoeckenius, W. Rhodopsin-Like Protein from the Purple Membrane of *Halobacterium halobium*. *Nature* **1971**, *233*, 149−152.

(2) Oesterhelt, D.; Stoeckenius, W. Functions of a New Photoreceptor Membrane. *Proc. Natl. Acad. Sci. U.S.A.* **1973**, *70*, 2853−2857.

(3) Luecke, H.; Schobert, B.; Richter, H. T.; Cartailler, J. P.; Lanyi, J. K. Structure of Bacteriorhodopsin at 1.55 Å Resolution. *J. Mol. Biol.* **1999**, *291*, 899−911.

(4) Henderson, R.; Baldwin, J. M.; Ceska, T. A.; Zemlin, F.; Beckmann, E.; Downing, K. H. Model for the Structure of Bacteriorhodopsin Based on High-Resolution Electron Cryo-Microscopy. *J. Mol. Biol.* **1990**, *213*, 899−929.

(5) Heyes, C. D.; El-Sayed, M. A. The Role of the Native Lipids and Lattice Structure in Bacteriorhodopsin Protein Conformation and Stability as Studied by Temperature-Dependent Fourier Transform-Infrared Spectroscopy. *J. Biol. Chem.* **2002**, *277*, 29437−29443.

(6) Bogomolni, R.; Baker, R.; Lozier, R.; Stoeckenius, W. Light-Driven Proton Translocations in *Halobacterium halobium*. *Biochim. Biophys. Acta, Bioenerg.* **1976**, *440*, 68−88.

(7) Stuart, J. A.; Birge, R. R. In *Biomembranes*; Lee, A. G., Ed.; JAI Press: London, 1996; Vol. 2A, pp 33−140.

(8) Balashov, S. P. Protonation Reactions and Their Coupling in Bacteriorhodopsin. *Biochim. Biophys. Acta, Bioenerg.* **2000**, *1460*, 75−94.

(9) Lozier, R. H.; Niederberger, W.; Bogomolni, R. A.; Hwang, S.; Stoeckenius, W. Kinetics and Stoichiometry of Light-Induced Proton Release and Uptake from Purple Membrane Fragments, *Halobacterium halobium* Cell Envelopes, and Phospholipid Vesicles Containing Oriented Purple Membrane. *Biochim. Biophys. Acta, Bioenerg.* **1976**, *440*, 545−556.

(10) Hampp, N.; Popp, A.; Bräuchle, C.; Oesterhelt, D. Diffraction Efficiency of Bacteriorhodopsin Films for Holography Containing Bacteriorhodopsin Wildtype BR$_{WT}$ and Its Variants BR$_{D85E}$ and BR$_{D96N}$. *J. Phys. Chem.* **1992**, *96*, 4679−4685.

(11) Hampp, N.; Thoma, R.; Zeisel, D.; Bräuchle, C.; Oesterhelt, D. Bacteriorhodopsin Variants for Holographic Pattern Recognition. *Adv. Chem.* **1994**, *240*, 511−526.

(12) Groma, G. I.; Bogomolni, R. A.; Stoeckenius, W. The Photocycle of Bacteriorhodopsin at High pH and Ionic Strength I. Effects of pH and Buffer on the Absorption Kinetics. *Biochim. Biophys. Acta, Bioenerg.* **1997**, *1319*, 59−68.

(13) Stuart, J. A.; Tallent, J. R.; Tan, E. H. L.; Birge, R. R. Protein-Based Volumetric Memories. *Proc. IEEE Nonvol. Mem. Tech. (INVMTC)* **1996**, *6*, 45−51.

(14) Stuart, J. A.; Marcy, D. L.; Birge, R. R. In *Bioelectronic Applications of Photochromic Pigments*; Dér, A., Keszthelyi, L., Eds.; IOS Press: Szeged, Hungary, 2000; Vol. 335, pp 30−43.

(15) Birge, R. R.; Gillespie, N. B.; Izaguirre, E. W.; Kusnetzow, A.; Lawrence, A. F.; Singh, D.; Song, Q. W.; Schmidt, E.; Stuart, J. A.; Seetharaman, S.; Wise, K. J. Biomolecular Electronics: Protein-Based

Associative Processors and Volumetric Memories. *J. Phys. Chem. B* **1999**, *103*, 10746−10766.

(16) Hampp, N. Bacteriorhodopsin: Mutating a Biomaterial into an Optoelectronic Material. *Appl. Microbiol. Biotechnol.* **2000**, *53*, 633−639.

(17) Hampp, N. Bacteriorhodopsin as a Photochromic Retinal Protein for Optical Memories. *Chem. Rev.* **2000**, *100*, 1755−1776.

(18) Tallent, J. R.; Stuart, J. A.; Song, Q. W.; Schmidt, E. J.; Martin, C. H.; Birge, R. R. Photochemistry in Dried Polymer Films Incorporating the Deionized Blue Membrane Form of Bacteriorhodopsin. *Biophys. J.* **1998**, *75*, 1619−1634.

(19) Greco, J. A.; Wagner, N. L.; Birge, R. R. Fourier Transform Holographic Associative Processors Based on Bacteriorhodopsin. *Int. J. Unconventional Comput.* **2012**, *8*, 433−457.

(20) Gillespie, N. B.; Wise, K. J.; Ren, L.; Stuart, J. A.; Marcy, D. L.; Hillebrecht, J.; Li, Q.; Ramos, L.; Jordan, K.; Fyvie, S.; Birge, R. R. Characterization of the Branched-Photocycle Intermediates P and Q of Bacteriorhodopsin. *J. Phys. Chem. B* **2002**, *106*, 13352−13361.

(21) Popp, A.; Wolperdinger, M.; Hampp, N.; Bräuchle, C.; Oesterhelt, D. Photochemical Conversion of the O-intermediate to 9-*cis*-Retinal-Containing Products in Bacteriorhodopsin Films. *Biophys. J.* **1993**, *65*, 1449−1459.

(22) Wagner, N. L.; Greco, J. A.; Ranaghan, M. J.; Birge, R. R. Directed Evolution of Bacteriorhodopsin for Applications in Bioelectronics. *J. R. Soc., Interface* **2013**, *10*, 20130197.

(23) Fischer, U. C.; Towner, P.; Oesterhelt, D. Light Induced Isomerization, at Acidic pH, Initiates Hydrolysis of Bacteriorhodopsin to Bacterio-Opsin and 9-*cis*-Retinal. *Photochem. Photobiol.* **1981**, *33*, 529−537.

(24) Turner, G. J.; Miercke, L. J. W.; Thorgeirsson, T. E.; Kliger, D. S.; Betlach, M. C.; Stroud, R. M. Bacteriorhodopsin D85N: Three Spectroscopic Species in Equilibrium. *Biochemistry* **1993**, *32*, 1332−1337.

(25) Tallent, J.; Song, Q. W.; Li, Z.; Stuart, J.; Birge, R. R. Effective Photochromic Nonlinearity of Dried Blue-Membrane Bacteriorhodopsin Films. *Opt. Lett.* **1996**, *21*, 1339−1341.

(26) Tittor, J.; Schweiger, U.; Oesterhelt, D.; Bamberg, E. Inversion of Proton Translocation in Bacteriorhodopsin Mutants D85N, D85T, and D85,96N. *Biophys. J.* **1994**, *67*, 1682−1690.

(27) Balashov, S. P.; Imasheva, E. S.; Govindjee, R.; Ebrey, T. G. Titration of Aspartate-85 in Bacteriorhodopsin: What it Says About Chromophore Isomerization and Proton Release. *Biophys. J.* **1996**, *70*, 473−481.

(28) Millerd, J. E.; Rohrbacher, A.; Brock, N. J.; Chau, C.-K.; Smith, P.; Needleman, R. Improved Sensitivity in Blue-Membrane Bacteriorhodopsin Films. *Opt. Lett.* **1999**, *24*, 1355−1357.

(29) Chang, C.-H.; Liu, S. Y.; Jonas, R.; Govindjee, R. The Pink Membrane: The Stable Photoproduct of Deionized Purple Membrane. *Biophys. J.* **1987**, *52*, 617−623.

(30) Chronister, E. L.; Corcoran, T. C.; Song, L.; El-Sayed, M. A. On the Molecular Mechanisms of the Schiff Base Deprotonation During the Bacteriorhodopsin Photocycle. *Proc. Natl. Acad. Sci. U.S.A.* **1986**, *83*, 8580−8584.

(31) Váró, G.; Lanyi, J. K. Photoreactions of Bacteriorhodopsin at Acid pH. *Biophys. J.* **1989**, *56*, 1143−1151.

(32) Moore, T.; Edgerton, M.; Parr, G.; Greenwood, C.; Perham, R. Studies of an Acid-Induced Species of Purple Membrane from *Halobacterium halobium*. *Biochem. J.* **1978**, *171*, 469−476.

(33) Cladera, J.; Galisteo, M. L.; Sabes, M.; Mateo, P. L.; Padros, E. The Role of Retinal in the Thermal Stability of the Purple Membrane. *Eur. J. Biochem.* **1992**, *207*, 581−585.

(34) Kresheck, G.; Lin, C.; Williamson, L.; Mason, W.; Jang, D.; El-Sayed, M. The Thermal Stability of Native, Delipidated, Deionized and Regenerated Bacteriorhodopsin. *J. Photochem. Photobiol., B* **1990**, *7*, 289−302.

(35) Okumura, H.; Murakami, M.; Kouyama, T. Crystal Structures of Acid Blue and Alkaline Purple Forms of Bacteriorhodopsin. *J. Mol. Biol.* **2005**, *351*, 481−495.

(36) Liu, S. Y.; Ebrey, T. G. The Quantum Efficiency for the Interphotoconversion of the Blue and Pink Forms of Purple Membrane. *Photochem. Photobiol.* **1987**, *46*, 263−267.

(37) Bazhenov, V. Y.; Soskin, M. S.; Taranenko, V. B. Holographic Recording by Continuous Illumination in a Suspension of Purple Membranes of Halobacteria. *Sov. Tech. Phys. Lett.* **1987**, *13*, 382−384.

(38) Gross, R. B.; Izgi, K. C.; Birge, R. R. Holographic Thin Films, Spatial Light Modulators, and Optical Associative Memories Based on Bacteriorhodopsin. *Proc. SPIE* **1992**, *1662*, 186−196.

(39) Landin, J. S.; Katragadda, M.; Albert, A. D. Thermal Destabilization of Rhodopsin and Opsin by Proteolytic Cleavage in Bovine Rod Outer Segment Disk Membranes. *Biochemistry* **2001**, *40*, 11176−11183.

(40) Galisteo, M.; Sanchez-Ruiz, J. Kinetic Study into the Irreversible Thermal Denaturation of Bacteriorhodopsin. *Eur. Biophys. J.* **1993**, *22*, 25−30.

(41) Kogelnik, H. Coupled Wave Theory for Thick Hologram Gratings. *Bell Syst. Tech. J.* **1969**, *48*, 2909−2947.

(42) Birge, R. R.; Fleitz, P. A.; Gross, R. B.; Izgi, J. C.; Lawrence, A. F.; Stuart, J. A.; Tallent, J. R. Spatial Light Modulators and Optical Associative Memories Based on Bacteriorhodopsin. *Proc. IEEE EMBS* **1990**, *12*, 1788−1789.

(43) Bunkin, F. V.; Vsevolodov, N. N.; Druzhko, A. B.; Mitsner, B. I.; Prokhorov, A. M.; Savranskii, V. V.; Tkachenko, N. W.; Shevchenko, T. B. Diffraction Efficiency of Bacteriorhodopsin and Its Analogs. *Sov. Tech. Phys. Lett.* **1981**, *7*, 630−631.

(44) Thoma, R.; Hampp, N.; Bräuchle, C.; Oesterhelt, D. Bacteriorhodopsin Films as Spatial Light Modulators for Nonlinear-Optical Filtering. *Opt. Lett.* **1991**, *16*, 651−653.

(45) Renner, T.; Hampp, N. Bacteriorhodopsin-Films for Dynamic Time Average Interferometry. *Opt. Commun.* **1993**, *96*, 142−149.

(46) Birge, R. R. Protein-Based Optical Computing and Memories. *Computer* **1992**, *25*, 56−67.

(47) Xi, B.; Tetley, W. C.; Marcy, D. L.; Zhong, C.; Whited, G.; Birge, R. R.; Stuart, J. A. Evaluation of Blue and Green Absorbing Proteorhodopsins as Holographic Materials. *J. Phys. Chem. B* **2008**, *112*, 2524−2532.

(48) Birge, R. R.; Izgi, K. C.; Stuart, J. A.; Tallent, J. R. Wavelength Dependence of the Photorefractive and Photodiffractive Properties of Holographic Thin Films Based on Bacteriorhodopsin. *Proc. Mater. Res. Soc.* **1991**, *218*, 131−140.

(49) Ranaghan, M. J.; Wagner, N. L.; Sandberg, M. N.; Birge, R. R. In *Optical Biomimetics: Materials and Applications*; Large, M., Ed.; Woodhead Publishing: Cambridge, UK, 2012, pp 20−78.

(50) Downie, J. D.; Timuçin, D. A.; Smithey, D. T.; Crew, M. Long Holographic Lifetimes in Bacteriorhodopsin Films. *Opt. Lett.* **1998**, *23*, 730−732.

(51) Lanyi, J. K.; Tittor, J.; Váró, G.; Krippahl, G.; Oesterhelt, D. Influence of the Size and Protonation State of Acidic Residue 85 on the Absorption Spectrum and Photoreaction of the Bacteriorhodopsin Chromophore. *Biochim. Biophys. Acta, Bioenerg.* **1992**, *1099*, 102−110.

(52) Mogi, T.; Stern, L. J.; Marti, T.; Chao, B. H.; Khorana, H. G. Aspartic Acid Substitutions Affect Proton Translocation by Bacteriorhodopsin. *Proc. Natl. Acad. Sci. U.S.A.* **1988**, *85*, 4148−4152.

(53) Mowery, P. C.; Lozier, R. H.; Chae, Q.; Tseng, Y. W.; Taylor, M.; Stoeckenius, W. Effect of Acid pH on the Absorption Spectra and Photoreactions of Bacteriorhodopsin. *Biochemistry* **1979**, *18*, 4100−4107.

(54) Richter, H.-T.; Brown, L. S.; Needleman, R.; Lanyi, J. K. A Linkage of the pKa's of Asp-85 and Glu-204 Forms Part of the Reprotonation Switch of Bacteriorhodopsin. *Biochemistry* **1996**, *35*, 4054−4062.

(55) Subramaniam, S.; Marti, T.; Khorana, H. Protonation State of Asp (Glu)-85 Regulates the Purple-to-Blue Transition in Bacteriorhodopsin Mutants Arg 82 to Ala and Asp 85 to Glu: The Blue Form Is Inactive in Proton Translocation. *Proc. Natl. Acad. Sci. U.S.A.* **1990**, *87*, 1013−1017.

(56) Richter, H. T.; Needleman, R.; Lanyi, J. K. Perturbed Interaction Between Residues 85 and 204 in Tyr185–>Phe and Asp85–>Glu Bacteriorhodopsins. *Biophys. J.* **1996**, *71*, 3392−3398.

(57) Jackson, M. B.; Sturtevant, J. M. Phase Transitions of the Purple Membranes of *Halobacterium halobium*. *Biochemistry* **1978**, *17*, 911−915.

(58) Muller, J.; Munster, C.; Salditt, T. Thermal Denaturing of Bacteriorhodopsin by X-Ray Scattering from Oriented Purple Membranes. *Biophys. J.* **2000**, *78*, 3208−3217.

(59) Wang, J.; El-Sayed, M. Temperature Jump-Induced Secondary Structural Change of the Membrane Protein Bacteriorhodopsin in the Premelting Temperature Region: A Nanosecond Time-Resolved Fourier Transform Infrared Study. *Biophys. J.* **1999**, *76*, 2777−2783.

(60) Wang, J.; El-Sayed, M. A. The Effect of Protein Conformation Change from αII to αI on the Bacteriorhodopsin Photocycle. *Biophys. J.* **2000**, *78*, 2031−2036.

(61) Cladera, J.; Galisteo, M.; Duñach, M.; Mateo, P.; Padrós, E. Thermal Denaturation of Deionized and Native Purple Membranes. *Biochim. Biophys. Acta, Biomembr.* **1988**, *943*, 148−156.

(62) Taneva, S. G.; Goni, F. M.; Tuparev, N. P.; Petkanchin, I.; Der, A.; Muga, A. Effect of Asp85 Replacement by Thr on the Conformation, Surface Electric Properties and Stability of Bacteriorhodopsin. *Colloids Surf., A* **2002**, *209*, 193−200.

(63) Dáncshazy, Z.; Tokaji, Z. Blue Light Regeneration of Bacteriorhodopsin Bleached by Continuous Light. *FEBS Lett.* **2000**, *476*, 171−173.

(64) Brouillette, C.; Muccio, D.; Finney, T. pH Dependence of Bacteriorhodopsin Thermal Unfolding. *Biochemistry* **1987**, *26*, 7431−7438.

(65) Pandey, P. C.; Upadhyay, B. C.; Pandey, C. M. D.; Pathak, H. C. Electrochemical Studies on D96N Bacteriorhodopsin and its Application in the Development of Photosensors. *Sens. Actuators, B* **1999**, *56*, 112−120.

(66) Hampp, N.; Bräuchle, C.; Oesterhelt, D. Bacteriorhodopsin Wildtype and Variant Aspartate-96 to Asparagine as Reversible Holographic Media. *Biophys. J.* **1990**, *58*, 83−93.

(67) Váró, G.; Lanyi, J. K. Kinetic and Spectroscopic Evidence for an Irreversible Step Between Deprotonation and Reprotonation of the Schiff Base in the Bacteriorhodopsin Photocycle. *Biochemistry* **1991**, *30*, 5008−5015.

2808

dx.doi.org/10.1021/am405363z | *ACS Appl. Mater. Interfaces* 2014, 6, 2799−2808